

Iterated Instabilities during Droplet Fission

Michael P. Brenner

Department of Mathematics, The University of Chicago, Chicago, Illinois 60637

X. D. Shi and Sidney R. Nagel

James Franck Institute and Department of Physics, The University of Chicago, Chicago, Illinois 60637

(Received 22 June 1994)

Recent observations indicate that the shape of a fluid interface undergoes repeated instabilities arbitrarily close to breakup. We interpret this behavior as the result of successive instabilities of the similarity solution of Eggers [Phys. Rev. Lett. **71**, 3458 (1993)]. We show that the similarity solution is unstable to finite amplitude perturbations, with critical amplitude going to zero at the singularity. Thermal fluctuations in the fluid can trigger the instabilities.

PACS numbers: 47.15.Hg, 03.40.Gc, 68.10.-m

The scientific study of droplet breakup has a distinguished history, beginning with the work of Lord Rayleigh in the late nineteenth century [1]. Recently there has been a rebirth of interest, largely motivated by questions about the singularity mechanism [2]. It was proposed that the interfacial shape near breakup is self-similar [3–8] and is essentially independent of experimental details. The physical reason for this is that near breakup the droplet radius becomes much smaller than any other length scale (given by initial conditions or external forcing), so that the shape of the interface becomes independent of these scales. Self-similarity has been observed in models for droplet breakup in a Hele-Shaw cell [4–6] and the rupture of soap films [7].

For three-dimensional fluid breakup, Eggers and Dupont [8,9] found a similarity solution describing both the thickness $h(z - z_0)$ and the velocity $v(z - z_0)$ of an axisymmetric fluid interface near a breakup at vertical coordinate z_0 . The solution has the form

$$h_E(z, t) = \ell_\eta t' H\left(\frac{z - z_0}{\ell_\eta t'^{1/2}}\right), \quad (1)$$

$$v_E(z, t) = \frac{\ell_\eta}{t_\eta} t'^{-1/2} U\left(\frac{z - z_0}{\ell_\eta t'^{1/2}}\right). \quad (2)$$

Here, ℓ_η ($\equiv \eta^2/\gamma\rho$) is the viscous length scale, t_η ($\equiv \eta^3/\gamma^2\rho$) is the viscous time scale, and η , ρ , and γ are, respectively, the fluid viscosity, density, and surface tension. $t' \equiv t^* - t/t_\eta$ is the dimensionless time to breakup. H and U contain no free parameters. The minimum thickness of the interface h_{\min} follows the universal law $h_{\min} = 0.03\ell_\eta t'$.

However, in a set of experiments and computer simulations [10], we showed that the singularity of viscous droplets falling from a faucet differs from the above scaling. Examples of interfacial shapes observed experimentally are shown in Fig. 1. Figure 1(a) shows a drop of an 85% glycerol in water mixture. Figure 1(b) shows a close-up near the breaking point, in which long necks are attached to thinner necks; at slightly higher viscos-

ity [Fig. 1(c)] regions of varicosity (called “blobs”) appear. Numerical simulations of hydrodynamic equations with a weak noise source reproduce these features of the experiments and also show that necks and blobs form repeatedly (on smaller and smaller scales) as the interface breaks [10]. These instability cascades are only observed for fluids with viscosity greater than about 1 P [11].

The purpose of this Letter is to present the instability mechanism and to compute the amount of noise necessary to produce necks and blobs. Our argument stems from the numerical observation (Fig. 2) that, immediately before a new neck forms, the thinnest section of the interface is well approximated by the similarity solution. The nonsteady singularity results from repeated instabilities of the similarity solution.

A static cylindrical interface [1] is unstable to modulations with wavelength larger than its circumference. Although near breakup the interface is neither cylindrical or static (e.g., the fluid velocity diverges), remnants of this Rayleigh instability still exist: On scales much smaller than the characteristic scale of the similarity solution $\ell_\eta t'^{1/2}$, the interface is *approximately* a cylinder with circumference of order $\ell_\eta t'$. Perturbations with wavelength λ satisfying $\ell_\eta t' \ll \lambda \ll \ell_\eta t'^{1/2}$ obey Rayleigh's stability criterion and will grow. Remarkably, the time scale for a Rayleigh instability on a cylinder of thickness h_{\min} [12] is $6h_{\min}t_\eta/\ell_\eta \approx t^* - t/6$, so that appreciable growth can occur in the short time before breakup.

These modes are *convected* and *stretched* as they grow; a generic perturbation moves away from the singularity, diminishing its effect. However, if a perturbation originates at a stagnation point, it remains near the singularity and can change the breakup [13]. Below, we show that perturbations of the interface with amplitude larger than $A_c = 10^{-4.7} t'^{1.5} h_{\min}$, a time distance t' from the singularity, produce observable changes in the breakup. This critical amplitude goes to zero at the singularity, so that even thermal fluctuations provoke instabilities. We find a viscosity dependence which is consistent with the experiments.

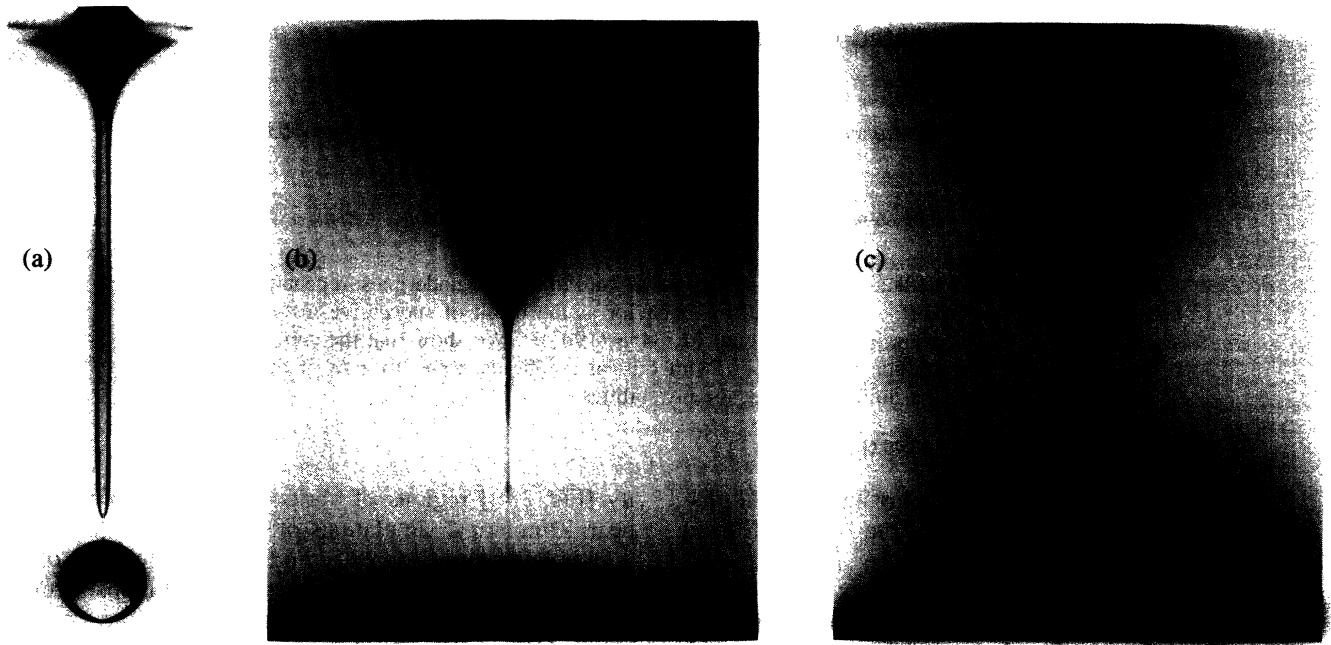


FIG. 1. (a) A drop of an 85% glycerol water mixture ($\eta = 1$ P) falling from a 2 cm diameter nozzle [10]. (b) A close-up near breakoff where long necks are attached to thinner necks. (c) Blobs develop near the breaking point for a slightly higher viscosity fluid (87% mixture $\eta = 1.4$ P).

Our analysis uses the slender body equations [9,14] for the interfacial thickness $h(z, t)$ and the fluid velocity $v(z, t)$, nondimensionalized using ℓ_η and t_η :

$$\partial_t h^2 = -(h^2 v)_z, \tag{3}$$

$$\partial_t v + v v_z = \frac{3}{h^2} (h^2 v_z)_z - \partial_z \left(\frac{1}{h} - h_{zz} \right). \tag{4}$$

These equations were derived from the Navier-Stokes equations for long-wavelength, axisymmetric disturbances.

We first find the local growth rate for perturbations on the similarity solution whose wavelength λ satisfies $\ell_\eta t' \ll \lambda \ll \ell_\eta t'^{1/2}$. Stability analysis is carried out in the rescaled frame of the similarity solution by taking $h = h_E + \ell_\eta t' g(\zeta, t')$ and $v = v_E + \frac{\ell_\eta}{t_\eta} t'^{-1/2} w(\zeta, t')$, where $\zeta \equiv z - z_0/\ell_\eta t'^{1/2}$ and where g and w are small perturbations of the similarity solution. To linear order,

$$\partial_\tau g - g + \left(U + \frac{\zeta}{2} \right) g_\zeta + \frac{H w_\zeta}{2} + H_\zeta w + \frac{U_\zeta}{2} g = 0, \tag{5}$$

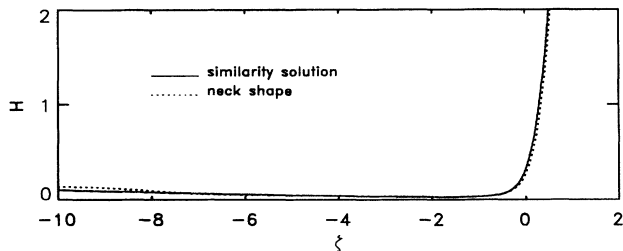


FIG. 2. Comparison between the shape of the third neck in the simulation of [10] and the similarity solution [8].

$$\begin{aligned} \partial_\tau w + \frac{w}{2} + \left(U + \frac{\zeta}{2} \right) w_\zeta + w U_\zeta - 3 w_{\zeta\zeta} - 6 \frac{U_\zeta g_\zeta}{H} \\ - 6 \frac{H_\zeta w_\zeta}{H} + 6 \frac{H_\zeta U_\zeta}{H^2} g - \frac{g_\zeta}{H^2} + 2 \frac{H_\zeta}{H^3} g \\ - t' g_{\zeta\zeta\zeta} = t' H_{\zeta\zeta\zeta}, \end{aligned} \tag{6}$$

where $\tau \equiv -\ln(t')$.

The local growth rate is computed by taking both g and w to be proportional to e^S , where $S(x, \zeta, \tau, \epsilon) \equiv \beta(\zeta, \epsilon)\tau + ik(\tau)x$ with $x \equiv \zeta/\epsilon$ and $\epsilon \ll 1$. Plugging this ansatz into Eqs. (5) and (6) and solving for S systematically in powers of ϵ gives to leading order [15]

$$\text{Im}(\beta) = - \left[\left(U + \frac{\zeta}{2} \right) k \right] \frac{1}{\epsilon}, \tag{7}$$

$$\text{Re}(\beta) = 1 + \frac{U_\zeta}{2} + \frac{1}{6H} [1 - t'(k/\epsilon)^2 H] - 3 \left(\frac{H_\zeta}{H} \right)^2, \tag{8}$$

$$\frac{k_\tau}{k} = -U_\zeta - \frac{1}{2}. \tag{9}$$

Equation (9) for $k(\tau)$ eliminates secular terms and has the simple physical interpretation that the wave number of a perturbation is stretched by the interfacial velocity $U_i = -\partial_k \text{Im}(\beta) = U + \zeta/2$ as it moves.

The local growth rate implies that if $A(\zeta_0)$ is the amplitude of a perturbation at ζ_0 , then approximating $\frac{d}{d\tau} \ln(A) \approx U_i \frac{d}{d\zeta} \ln(A) = \text{Re}(\beta)$ [16] gives

$$\frac{A(\zeta)}{A(\zeta_0)} = \exp \left(\int_{\zeta_0}^{\zeta} \frac{d\zeta}{U_i} \text{Re}(\beta) \right), \tag{10}$$

where $\zeta(\tau)$ solves $\zeta_\tau = U_i$. Maximal growth occurs for perturbations originating near the point ζ^* , where $U_i = U(\zeta^*) + \zeta^*/2 = 0$. Perturbations starting near ζ^* move slowly and thus have more time to grow. Remarkably, $H(\zeta^*)$ differs by only a fraction of a percent from the absolute minimum of H , so the local growth rate near ζ^* is nearly the maximal growth rate.

A perturbation originating near ζ^* undergoes rapid growth and stretching, continuing until it reaches $\zeta_- \approx -10$ (if it starts on the left of η^*) or $\zeta_+ \approx -0.5$ (if it starts on the right). Beyond these points there is not appreciable growth in the laboratory frame. Analysis of the local growth rate shows that perturbations originating for $\zeta > \zeta^*$ are damped [17]. Depending on their initial amplitude, perturbations starting with $\zeta < \zeta^*$ become either (1) a *blob*, which distorts the shape of the interface, or (2) a *neck*, which also changes the spatial and temporal location of the singularity. In either case, numerical simulations indicate that the shape of the interface relaxes to a similarity solution. Instabilities in the similarity solution can be generated indefinitely, leading to the rough singularity of [10].

The largest growth occurs when a perturbation with wavelength of order h_{\min} ($t'^{1/2}$ in rescaled units) originates at ζ^* . Using (10) we find that $A(\zeta_-)/A(\zeta_0) \sim t'^{-p}$ where p depends on local derivatives of the similarity solution evaluated at ζ^* . In order for $A(\zeta_-) \sim 0.03$ (the minimum neck thickness), $A(\zeta_0)$ must be larger than the critical amplitude

$$A_c \approx 0.03\alpha t'^p, \quad (11)$$

where the constants $p = 1.49$ and $\alpha = 10^{-4.7}$ are determined using the numerical values of the similarity solution [8]. Note that (11) is written in *rescaled units*.

We have compared numerical solutions of the linearized Eqs. (5) and (6) to Eq. (10), with excellent agreement [17]. Moreover, simulations of Eqs. (3) and (4) verify our basic predictions. Figure 3(a) shows a simulation (initially $t' = 10^{-4}$) in which a perturbation with size 10^{-13} ($= 10^{-8}h_{\min}$) and wavelength of order h_{\min} was placed on the interface very close to ζ^* . The perturbation grows very rapidly and changes both the spatial and temporal locations of the singularity, forming a “neck.” The solution near the new breaking point approaches a similarity solution. Figure 3(b) shows a simulation (initially $t' = 0.3$) in which a much larger bump (size $10^{-10} = 10^{-5}h_{\min}$) with wavelength of order h_{\min} begins farther from ζ^* . Here, the growth is not sufficient to change the location of the rupture, but does form a blob. By repeating such simulations for perturbations of different amplitudes, we estimate numerically the critical amplitude A_c . For $t' = 0.3$, 0.03 , and 10^{-4} , the numerical upper bounds for the critical amplitudes are $10^{-5.5}$, $10^{-6.9}$, and 10^{-10} , respectively, in agreement with (11).

Since the analysis is nondimensional, instabilities occur independently of fluid parameters (as long as sufficient noise is present). However, the *scale* at which instabilities

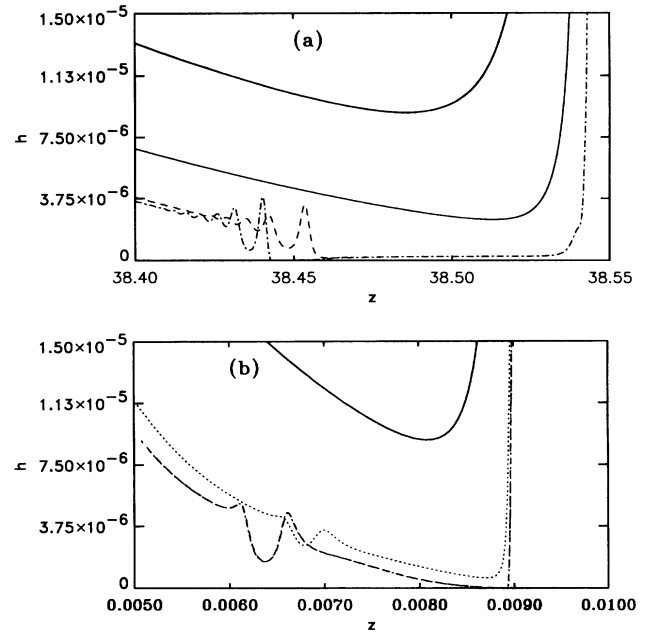


FIG. 3. (a) The solid line is the first time, where a bump of size 10^{-13} is placed at the stagnation point of the similarity solution. The dotted, dashed, and dot-dashed lines represent three subsequent times. (b) A bump of size 10^{-10} is placed on the similarity solution farther from the stagnation point.

set in depends on the fluid, because the interface must be approximated by the similarity solution, requiring $t' \ll 1$. Thus when studying the interfacial shape at a fixed radius, instabilities occur when ℓ_η is much larger than the radius. This agrees with the experimental viscosity dependence [10]. The characteristic size of the structures forming at a given time before breakoff is given by the characteristic length scale of the similarity solution, also in agreement with our observations.

Without an external noise source, simulations do not show repeated instabilities. However, given that Eqs. (3) and (4) only *approximate* the full Navier-Stokes equations, external noise may be unnecessary. For experiments, this is irrelevant, because there are many unavoidable types of external noise. The most ubiquitous are thermal fluctuations, which produce, for example, capillary waves on the interface. These fluctuations have a significant effect when their amplitude exceeds the threshold amplitude given by Eq. (11). The result shows [17] that thermal capillary waves produce instabilities whenever the droplet radius goes below the threshold

$$h_{\text{thres}} \sim \ell_\mu \left(\frac{\ell_T}{\ell_\mu} \right)^{2/5}, \quad (12)$$

where $\ell_T = \sqrt{k_B T / \gamma}$. Using the parameters appropriate for the experiments shown in Fig. 1 gives $h_{\text{thres}} \sim 1 \mu\text{m}$ [18]. This seems too small to explain Fig. 1; other sources of noise must affect the experiments.

Finally, the effects of noise are not relegated to the vicinity of the singularity but can affect the gross shape as

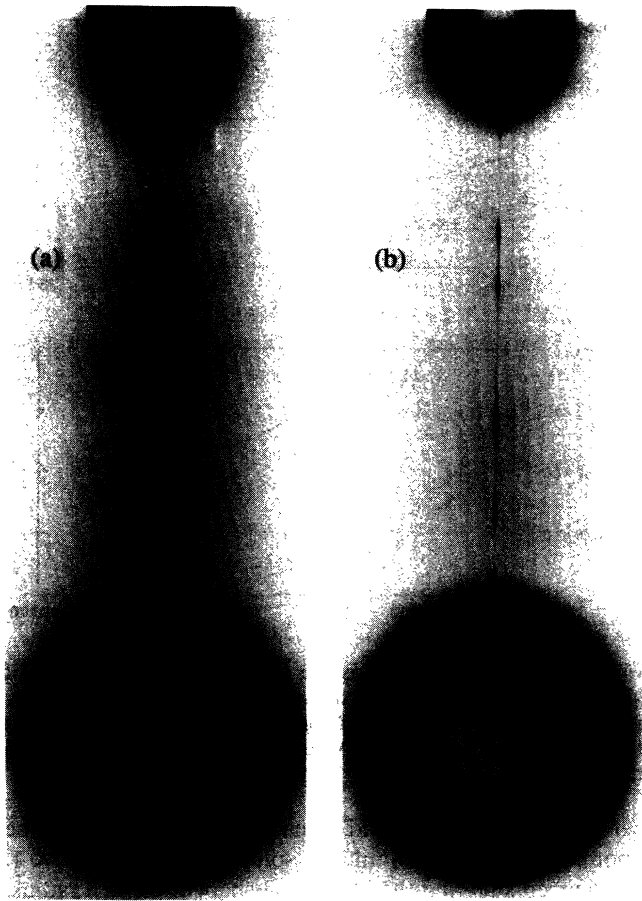


FIG. 4. A drop of 92% glycerol water mixture ($\eta = 2.8$ P) falling from a 2 mm diameter nozzle. Both the positions and the number of blobs vary between the two photographs.

well. In Fig. 4 we show pictures of the shape of a higher viscosity drop, demonstrating that both the number and location of the blobs vary when the experiment is repeated. A theoretical understanding of the noise sensitivity at such an early stage is currently lacking.

In conclusion, we have presented the mechanism for the instability cascades observed in experiments and simulations [10]. Even though velocity gradients diverge at breakoff, there is still sufficient time for instabilities to develop and change the location of the breaking point. Thermal fluctuations, whose relative size goes to zero at breakoff, can trigger instabilities. Since the theory only depends on Eggers' [8] universal similarity solution and the presence of thermal noise, instabilities will form during the breakup of any three-dimensional viscous fluid in vacuum, in any experimental situation. Many issues are left open: for example, what are the implications of the repeated instabilities for the satellite drop distribution after breakup?

We have benefited from discussions and collaborations with Leo Kadanoff, Jens Eggers, Todd Dupont, Andrea Bertozzi, Greg Forest, and Sergei Esipov. This research was supported by NSF DMR-MRL 88-19860, DOE DE-

FG02-92ER25119, NSF DMR 91-11733, and NSF DMR 9115595.

- [1] W. S. Rayleigh, Proc. London Math. Soc. **4**, 10 (1878).
- [2] H. A. Stone and L. G. Leal, J. Fluid Mech. **198**, 399 (1989); H. A. Stone, B. J. Bentley, and L. G. Leal, J. Fluid Mech. **173**, 131 (1986); M. Tjahjadi, H. A. Stone, and J. M. Ottino, J. Fluid Mech. **243**, 297 (1992).
- [3] J. Keller and M. J. Miksis, SIAM J. Appl. Math. **43**, 268 (1983); D. H. Peregrine, G. Shoker, and A. Symon, J. Fluid Mech. **212**, 25 (1990).
- [4] P. Constantin, T. F. Dupont, R. E. Goldstein, L. P. Kadanoff, M. J. Shelley, and S. M. Zhou, Phys. Rev. E **47**, 4169 (1993); T. F. Dupont, R. E. Goldstein, L. P. Kadanoff, and S. M. Zhou, Phys. Rev. E **47**, 4182 (1993).
- [5] R. E. Goldstein, A. I. Pesci, and M. J. Shelley, Phys. Rev. Lett. **70**, 3043 (1993).
- [6] A. L. Bertozzi, M. P. Brenner, T. F. Dupont, and L. P. Kadanoff, in *Trends and Perspectives in Applied Mathematics*, edited by L. Sirovich, Applied Mathematical Sciences Vol. 100 (Springer-Verlag, New York, 1994), p. 155.
- [7] M. Cryer and P. Steen, J. Colloid Interface Sci. **154**, 276 (1992).
- [8] J. Eggers, Phys. Rev. Lett. **71**, 3458 (1993); J. Eggers (to be published).
- [9] J. Eggers and T. F. Dupont, J. Fluid Mech. **262**, 205 (1994).
- [10] X. D. Shi, M. P. Brenner, and S. R. Nagel, Science **265**, 219 (1994).
- [11] These instabilities have now also been observed in recent cellular automata studies (M. Cieplak, M. S. Li, and J. R. Banavar), as well as jet experiments (T. A. Kowalewski, unpublished) and drop experiments (D. Henderson and W. Pritchard, unpublished).
- [12] S. Chandrasekhar, *Hydrodynamic and Hydromagnetic Stability* (Clarendon Press, Oxford, 1961).
- [13] The issues regarding the stability of the similarity solution are similar to those encountered in the stability of fingers in a Hele-Shaw cell [cf. D. Bensimon *et al.*, Rev. Mod. Phys. **58**, 977 (1986)] and the Ivanov parabola of dendritic growth [cf. D. Kessler *et al.*, Adv. Phys. **37**, 255 (1988)].
- [14] S. Bechtel, J. Cao, and M. G. Forest, J. Non-Newtonian Fluid Mech. **41**, 201 (1992).
- [15] Equations (5) and (6) contain explicit t' dependence because the similarity solution is not an exact solution of Eqs. (3) and (4). For long-wavelength perturbations, these terms are $O(t')$ and can be safely neglected. However, for short wavelengths ($\lambda \ll \ell_\eta t'$) the $t'g_{zzz}$ term dominates, causing perturbations to be damped. We have included the leading order term in t' in (8) in order to demonstrate the physically important damping effect.
- [16] Ya. B. Zeldovich, A. G. Istatov, N. I. Kidin, and V. B. Librivitch, Comb. Sci. Tech. **24**, 1 (1980).
- [17] M. P. Brenner (unpublished).
- [18] Note that the instabilities will be observable at a thickness smaller than h_{thres} , because the interface thins as the instability develops.

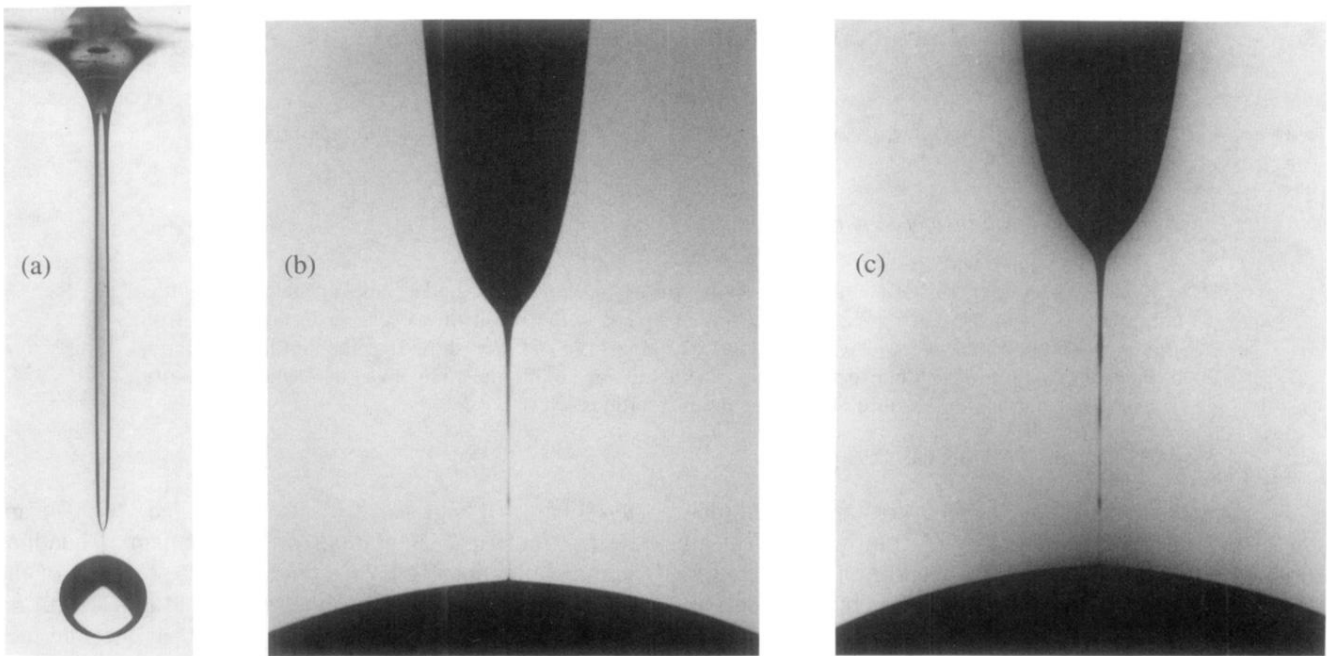


FIG. 1. (a) A drop of an 85% glycerol water mixture ($\eta = 1$ P) falling from a 2 cm diameter nozzle [10]. (b) A close-up near breakoff where long necks are attached to thinner necks. (c) Blobs develop near the breaking point for a slightly higher viscosity fluid (87% mixture $\eta = 1.4$ P).

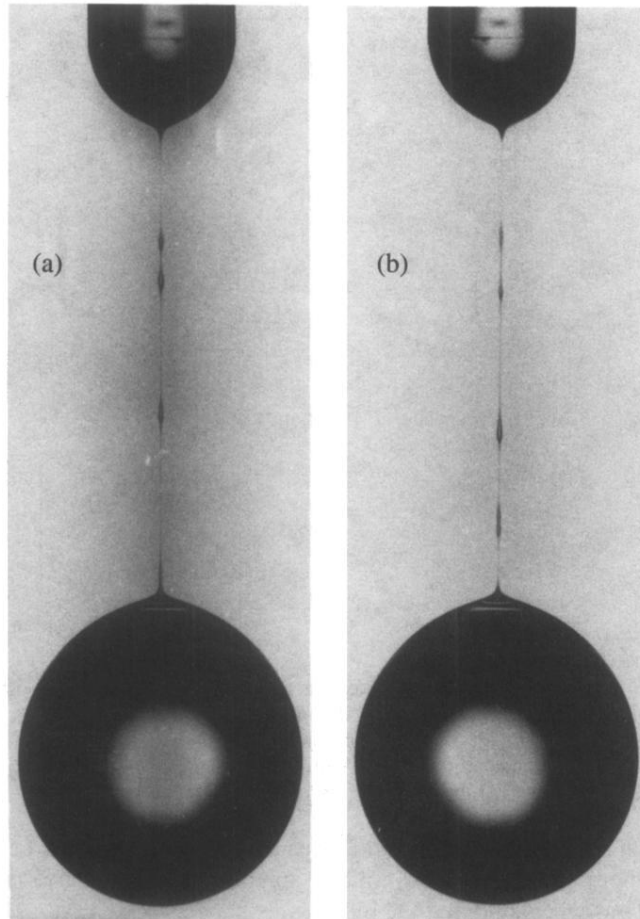


FIG. 4. A drop of 92% glycerol water mixture ($\eta = 2.8$ P) falling from a 2 mm diameter nozzle. Both the positions and the number of blobs vary between the two photographs.